Journal of Applied Physics ARTICLE scitation.org/journal/jap

Surface switching of mixed polyelectrolyte brushes made of 4-arm stars and linear chains: MD simulations

Cite as: J. Appl. Phys. **127**, 074301 (2020); doi: 10.1063/1.5130643
Submitted: 9 October 2019 · Accepted: 26 January 2020 ·
Published Online: 18 February 2020

View Online Export Citation CrossMark

Shaoyun Wang and Chaohui Tong[a)]

AFFILIATIONS

Department of Physics, School of Physical Science and Technology, Ningbo University, Ningbo, Zhejiang 315211, China

Note: This paper is part of the Special Topic on Polymer-Grafted Nanoparticles.

[a)]**Author to whom correspondence should be addressed:** tongchaohui@nbu.edu.cn

ABSTRACT

Using Langevin dynamics simulation, we study the surface switching properties of mixed polyelectrolyte brushes made of 4-arm stars and linear chains. The length and average charge fraction of the linear chains, Bjerrum length (a characteristic length to quantify the strength of the electrostatic interaction), the solvent quality as well as external electric fields were used as controlling parameters to induce sharp transitions of molecular conformations, leading to brush surfaces dominated by end monomers of linear chains or stars. Phase diagrams in terms of the length and charge fraction of linear chains demarcating different regimes of the composition of brush surfaces were constructed under different external electric fields. Besides the different regimes in the phase diagram of mixed brushes under a stretching electric field or in the absence of electric fields, a new regime, which is featured by the linear chains with very low charge fraction sandwiched between the collapsed and un-collapsed stars, emerges in the phase diagram under a collapsing electric field. The stratification within the brush layer of the mixed brushes under external electric fields was also investigated.

I. INTRODUCTION

Polymer brushes, monolayers of polymer chains densely end-grafted to solid substrates, can modify surface properties and act as smart surface layers with a wide range of technological applications.[1–16] In recent years, experimental, theoretical, and computational studies of polymer brushes are no longer limited to polymer brushes made of linear chains; the research focus is shifted to polymer brushes made of branched chains, e.g., dentrons.[17–33] Branched polymer brushes can mediate the interactions between surfaces in an architecture-dependent manner and lead to improved physical/chemical properties of modified substrates compared to linear polymer brushes.[22,23] Branched polymer brushes possess a large number of terminal groups, which are accessible for chemical modifications. Thus, they have great potential for sensing and actuating in chemical and biological applications.

In stark contrast to monodisperse brushes made of linear chains, branched polymer brushes are composed of molecules with qualitatively different conformations in which a certain fraction of molecules retract into a very weakly stretched state rather than backfold, leading to the emergence of stratification inside the brush layers. This partition of the molecular ensemble into distinct layers normal to the grafting substrate has been confirmed by lattice self-consistent field (SCF) and molecular dynamics (MD) simulations.[19,21,26,27] Different theoretical models such as boxlike mean field model and analytical SCF model have been developed to analyze the stratification of starlike polymer brushes in the nonlinear elasticity regime.[21,24,27]

Similar to polymer brushes made of linear chains, the terminal groups of branched polymer brushes distribute throughout the brush layer. Thus, a certain fraction of terminal groups of branched polymer brushes are buried deep within the brush layer, rendering them inaccessible for chemical modification or inactive for sensing and actuating. It has been proposed that the addition of relatively short grafted linear chains to branched polymer brushes, which reside near the grafting substrate, can push the terminal groups of grafted branched chains to the periphery of the brush layer as desired for chemical modification or sensing/actuating.[31–33] Therefore, the study of mixed brushes made of branched chains and linear chains is of scientific and technological importance.

Polotsky and co-workers investigated the structure of mixed brushes made of arm-grafted polymer stars and linear chains using the Scheutjens–Fleer SCF calculation.[31] As expected, a segregation of linear and star macromolecules in the direction perpendicular to the grafting substrate emerges. Conformations of stars and linear chains in the brush were shown to be determined by the overall molecular weights and the longest path lengths of these two different types of polymer chains. The most interesting finding of their research is that when the linear chains have larger longest path but lower molecular weight than the stars, the conformations of grafted stars and linear chains essentially depend on the brush composition. When the fraction of linear chains is small, the terminal groups of linear chains reside on the periphery of the brush layer. Conversely, when the fraction of linear chains is large, the terminal groups of stars reside on the periphery of the brush layer. Using numerical lattice SCF and analytical SCF methods, Polotsky, *et al.* further studied the so-called "coil-to-flower" conformational transition in a single "minority" linear polymer chain inserted into a polymer brush made of star macromolecules perturbed by either the length of the linear chain or the brush grafting density.[32] In the "coil" state, the linear chain is immersed inside the brush. In the "flower" state, the upper part of the linear chain extrudes above the brush layer with the rest part of the chain strongly stretched. Using MD simulations, Su *et al.* investigated the structural properties of mixed brushes made of 4-arm stars and linear chains in order to explore the potential of such type of mixed brushes for the design of switched surfaces.[33] It was found from simulations that the length of grafted linear chains, which serves as a controlling parameter, can induce a sharp transition of the molecular conformations when exceeding a critical value. A phase diagram in terms of the length of linear chains and grafting density was constructed to display which one of the two different terminal groups is dominant on the periphery of the brush layer. Furthermore, the effect of solvent quality on the conformations of grafted stars and linear chains was also examined.

Nevertheless, the above theoretical and computational studies of mixed polymer brushes made of star and linear chains are limited to the case of neutral brushes, and the charged counterparts were not explored. The conformational behaviors of mixed brushes made of charged star and linear chains are much richer than their neutral counterparts due to the long-range nature of Coulomb interactions. Mixed polyelectrolyte (PE) brushes can respond to a wider range of external stimuli than their neutral counterparts, such as salt ions with different charge valences and concentrations, solution pH, and external electric fields. Therefore, mixed polyelectrolyte brushes made of star and linear chains are superior to neutral mixed brushes in designing smart surfaces for technological applications. This is why we embarked on the study of ionic (charged) mixed brushes made of star and linear chains.

In this work, by performing Langevin Dynamics (LD) simulations, we study the conformations and stratification of mixed brushes made of charged linear chains and stars. To explore the potential of these systems for the design of switchable "smart" surfaces for sensing and actuating, the length and average charge fraction of the linear chains, Bjerrum length, solvent quality as well as external electric fields were used as controlling parameters to create brush surfaces dominated by end monomers of either linear chains or stars. Phase diagrams in terms of the length and charge fraction of linear chains demarcating different regimes of the composition of brush surfaces were constructed under different external electric fields.

II. MODEL AND METHOD

In this study, the mixed polyelectrolyte brushes were set up as an ensemble of $Q = 66$ flexible 4-arm stars and linear chains randomly grafted on a planar solid substrate with dimensions $L_x \times L_y$ (xy plane) situated at $z = 0$. A second planar wall at $z = L_z$ closes the system with periodic boundary conditions applied only in the x and y directions. The grafting density of the mixed brush is given by $\sigma_g = Q/(L_x L_y)$. In the brush system, there are Q_S grafted 4-arm star macromolecules and Q_L grafted linear chains with $Q_S + Q_L \equiv Q$. The ratio of Q_L to Q was defined as a controlling parameter R_α determining the degree of substitution of stars by linear macromolecules (the fraction of stars is $1 - R_\alpha$). Note that the limits of $R_\alpha = 0$ and $R_\alpha = 1$ correspond to one-component brushes. The star and linear chains were created by a coarse-grained bead-spring model. Neutral and charged monomers as well as counterions were modeled as spherical Lennard-Jones (LJ) beads (σ, ε) with equal mass m and diameter σ. The connectivity between two neighboring monomers in the same polymer chain is maintained by the finitely extensible nonlinear elastic (FENE) bond potential. The end monomers of 4-arm stars and linear chains were randomly and homogeneously anchored on the square lattice at $z = 0$. For 4-arm stars, each arm consists of $N_{ms} = 50$ monomer units, leading to a molecular weight of 200 (in units of m) and a longest path length $L_{lp} = 100$ (in units of σ). The charge fraction of 4-arm stars f_s was fixed as $f_s = 1/3$ in the simulations; that is, every third monomer in each arm of a star macromolecule carries a negative charge (in units of elementary electronic charge). Each linear chain is made of N_{ml} monomer units with $N_{ml} \in \{100, 115, 125, 135, 150\}$. The charge fraction of linear chains f_l was varied with $f_l \in \{1/3, 1/4, 1/6, 1/8, 1/24\}$. In a linear chain, a total of $N_{ml}f_l$ monomers each carrying a negative charge are uniformly distributed along the chain. Each negatively charged monomer in 4-arm stars and linear chains releases one monovalent counterion into the salt-free aqueous solution sandwiched between the two walls. In LD simulations, water was treated as an uniform dielectric medium with a dielectric constant of 78 at the room temperature. An external electric field $\vec{E}$ was applied along the z direction, which exerts an electric force $eq\vec{E}$ on a charged particle (e stands for an elementary charge and $q = \pm 1$ for counterions and charged monomers, respectively).

All particles interact with each other through a truncated and shifted Lennard-Jones (LJ) potential. The grafted chains were thus assumed to be immersed in a good solvent. Both walls were modeled by a 12/6 Lennard-Jones wall potential. The long-range Coulomb interaction was calculated using the Smooth Particle Mesh Ewald method (SPME) with an approximate root mean square (rms) force error of 10^{-3}.[34] Because the periodic condition is broken in the z direction for the present star-polymer brush system, the Ewald sum was calculated in an extended system, which periodically repeats the original slab system in the z direction with the insertion of an empty space whose length is $2 \times L_z$ between them.[35] Furthermore, a correction term was added to the Coulomb potential. The methodological detail is provided in Sec. I of the supplementary material.

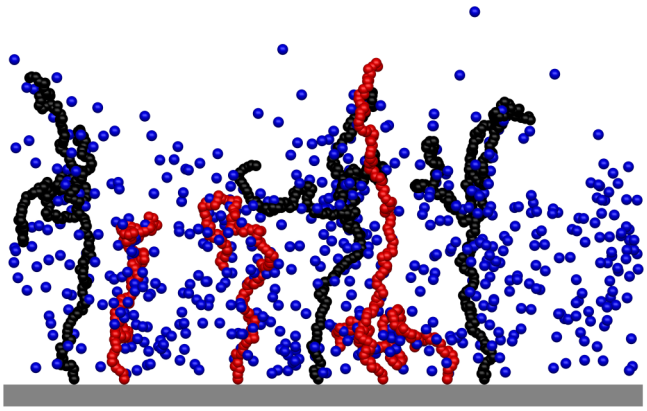

FIG. 1. A snapshot of a fraction of the simulation box ($-L_x/10 \le x \le L_x/10$, $-L_y/2 \le y \le L_y/2$, $0 \le z \le 75\sigma$) in the absence of external electric fields. The blue, red, and black spheres represent counterions, monomers of linear chains, and monomers of 4-arm star chains, respectively. The system parameters are $\sigma_g = 0.005\sigma^{-2}$, $R_\alpha = 0.5$, $N_{ms} = 50$, $N_{ml} = 100$, and $f_l = f_s = 1/3$.

The time evolution of the system is described by a standard Langevin dynamics. The temperature of the system is $k_BT = 1.2\varepsilon$ with ε denoting the amplitude of the LJ potential,[36] and the friction coefficient $\zeta = 1.0m\tau^{-1}$ with the time unit $\tau = \sigma(m/\varepsilon)^{1/2}$.[36,37] For an aqueous solution at the room temperature, Bjerrum length $\lambda_B = 0.71$ nm. In this study, we set $\lambda_B = 3\sigma$.[36,37] Thus, $\sigma \approx 0.24$ nm, which is approximately equal to the bond length of Polystyrene Sulfonate (PSS).[38] The LD unit of the external electric field is $\varepsilon/(e\sigma) = k_BT/(1.2e\sigma) \cong 9.0 \times 10^7$ V/m. In this work, the electric field strength was explored up to $|\vec{E}| = 1.0$ corresponding to 9.0×10^7 V/m. The maximum strength of applied electric fields is consistent with experimental observations.[39] In this work, the dimensionless grafting density $\sigma_g^* \equiv \sigma_g\sigma^2$ was explored from 0.001 up to 0.1. Furthermore, in this study, the vertical distributions of all the monomers $\phi(z)$, branching points of star $\phi^s_{branch}(z)$, end monomers of linear chains $\phi^l_{end}(z)$ and stars $\phi^s_{end}(z)$, charged monomers $\phi_{ch}(z)$, and counterions $\phi_{ion}(z)$ were investigated. All these distributions were normalized such that $\int_0^{L_z} P(z)\,dz = 1$, where $P(z)$ stands for either $\phi(z)$, $\phi^l_{end}(z)$, $\phi^s_{end}(z)$, $\phi^s_{branch}(z)$, $\phi_{ch}(z)$, or $\phi_{ion}(z)$.

The positions and velocities of all particles were updated by the Verlet algorithm with an integration time step of $\delta t = 0.005\tau$. It took 5×10^6 time steps to bring the initial system into an equilibrium state, followed by a production run phase. The data for each ensemble were computed by averaging over 1.5×10^7 time steps, during which a trajectory of 15 000 configurations were stored for the subsequent data analysis. A snapshot of the brush system under external electric fields is shown in Fig. 1.

III. RESULTS AND DISCUSSIONS

A. Mixed brushes in the absence of external electric fields

To explore the potential of mixed brushes made of branched and linear polyelectrolyte chains for the design of switchable surfaces, the chain length and average charge fraction of grafted linear chains were selected as the controlling parameters. Through analyzing the probability distributions of free end monomers of grafted stars and linear chains (see Fig. 2), we constructed a phase diagram in terms of the length and average charge fraction of grafted linear chains, which displays the dominant species on the brush surface, as shown in Fig. 3. The lower left region of the diagram corresponds to mixed brushes with relatively short chain length and low charge fraction of the linear chains, where the end monomers of grafted stars dominate the brush surface and grafted linear chains reside at the bottom of the brush layer. By contrast, the upper right region of the phase diagram shows that the end monomers of grafted linear chains with long chain length and high charge fraction dominate the brush surface. In between, there exists a relatively narrow regime in which the brush surface exhibits a mixture of end monomers of both species.

Previous numerical self-consistent field study showed that for neutral mixed brushes made of star and linear chains in the high grafting density regime, if the linear chains have larger longest path but lower molecular weight than the stars, the conformations of mixed brushes depend essentially on the brush composition. When the fraction of linear chains is small, the brush surface is dominated by the end monomers of linear chains. On the contrary, if the fraction of linear chains is large, the end monomers of stars dominate the brush surface. However, in the parameter range explored in this study with four grafting densities, i.e., $0.001\,\sigma^{-2}$, $0.005\,\sigma^{-2}$, $0.01\,\sigma^{-2}$, and $0.1\,\sigma^{-2}$, the interesting phenomenon of the dependence of the conformations of neutral mixed brushes on the brush

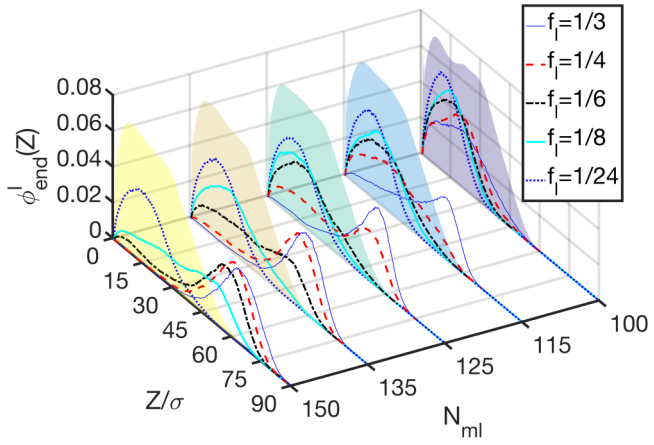

FIG. 2. Normalized probability distributions of free end monomers of grafted linear chains with different chain lengths and charge fractions. In the figure, the overall monomer probability distributions of mixed brushes are shown as the edges of shaded regions. The distributions of all of the monomers are for aiding the identification of the dominant species on the brush surface only and are thus not normalized. Because the overall monomer distribution is not very sensitive to the charge fraction of linear chains, the overall monomer distribution at $f_l = 1/4$ was chosen to approximate the overall distribution at each chain length. The grafting density and degree of substitution in the simulations are $\sigma_g = 0.005$, $R_\alpha = 0.5$.

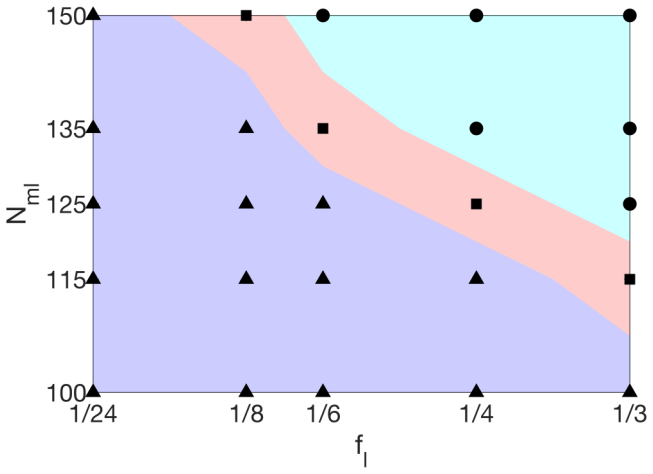

FIG. 3. Phase diagram in terms of the chain length and average charge fraction of linear chains depicting different regimes in which end monomers of different species dominate the brush surface. Triangles and filled circles indicate the dominance of end monomers of grafted stars and linear chains on the brush surface, respectively. Squares correspond to the ideally mixed phase.

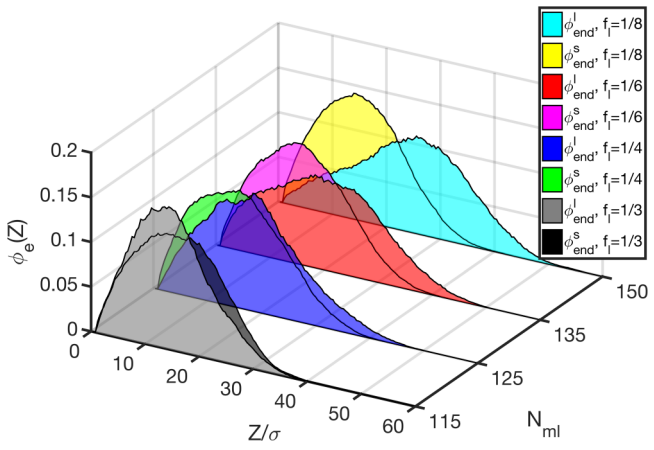

FIG. 4. Probability distributions of free end monomers of grafted linear chains and star chains with different chain lengths and charge fractions of linear chains under the condition of $\lambda_B = 10\sigma$. The linear chain lengths and average charge fractions in the figure correspond to the four phase points in the ideally mixed phase shown in Fig. 3. The grafting density and degree of substitution of stars by linear chains in the simulations are, respectively, $\sigma_g = 0.005$, $R_\alpha = 0.5$.

composition was not observed for the charged counterpart. Nevertheless, due to the very limited parameter space explored in this study, the existence of the unique dependence of the conformations of mixed charged brushes made of linear and star chains on the brush composition cannot be ruled out.

B. Effect of Bjerrum length on the phase diagram of mixed brushes in the absence of external electric fields

The electrostatic interaction between charged monomers and the released counterions exerts great influence on the chain conformations of polyelectrolyte brushes. Bjerrum length is a quantitative measure of the strength of electrostatic energy relative to the thermal energy. Simulation results revealed that a larger Bjerrum length, i.e., $\lambda_B = 10\sigma$, results in the collapse of the mixed PE brushes. By comparing Fig. 4 with Fig. 2, it can be found that the probability density distributions of the free end monomers of both star and linear chains shift downwards when Bjerrum length is increased from 3σ to 10σ. The collapse of the mixed PE brushes under the influence of a larger Bjerrum length is due to the strong counterion condensation. According to Manning's theory, the effective linear charge density or charge fraction of PE chains should be reduced to roughly σ/λ_B if the charge fraction of PE chains is larger than σ/λ_B because of the condensation of counterions on the oppositely charged monomers. Therefore, an increase of Bjerrum length leads to the decrease of mobile counterion concentration and the osmotic pressure inside the brush layer, thus the collapse of PE brushes. It can be seen from Figs. 4 and S1 in the supplementary material that the probability density profiles and average heights of the free end monomers of 4-arm stars with a fixed charge fraction of 1/3 are barely affected by the increase of chain length and reduction of charge fraction of linear chains under $\lambda_B = 10\sigma$. Thus, the grafted stars remain in the collapsed state. On the other hand, with the decrease of the average charge fraction of grafted linear chains, the degree of counterion condensation at $\lambda_B = 10\sigma$ also decreases for linear chains. A charge fraction of 1/8 deviates not much from the effective charge fraction of 1/10 estimated by Manning's theory for rodlike chains at the condition of $\lambda_B = 10\sigma$. Therefore, the probability density profiles of the free end monomers of grafted linear chains shift upwards with increasing chain length and decreasing charge fraction, as shown in Fig. 4. Figures 4 and S1 in the supplementary material clearly show that the two upper phase points in the ideally mixed phase at $\lambda_B = 3\sigma$ (see Fig. 3) will fall into the phase corresponding to the brush surface dominated by the free end monomers of linear chains at $\lambda_B = 10\sigma$. Therefore, a strong increase in Bjerrum length will result in a counterclockwise rotation of the region of its position of the ideally mixed phase in the phase diagram shown in Fig. 3.

We have also investigated the effect of shorter Bjerrum lengths, e.g., $\lambda_B = 2\sigma$, 1σ, and 0.5σ. Simulation results revealed that the ideally mixed state at $\lambda_B = 3\sigma$ remains unchanged with decreasing Bjerrum length (see Figs. S2 and S3 in the supplementary material). The scenario of very low Bjerrum length was not investigated because the grafting densities examined in this work are relatively low, under which the grafted star/linear chains would be in the mushroom region due to the very weak electrostatic interaction.

C. Effect of solvent quality on the phase diagram of mixed brushes in the absence of external electric fields

In this work, all of the simulations except those presented in this subsection were performed under the good solvent condition

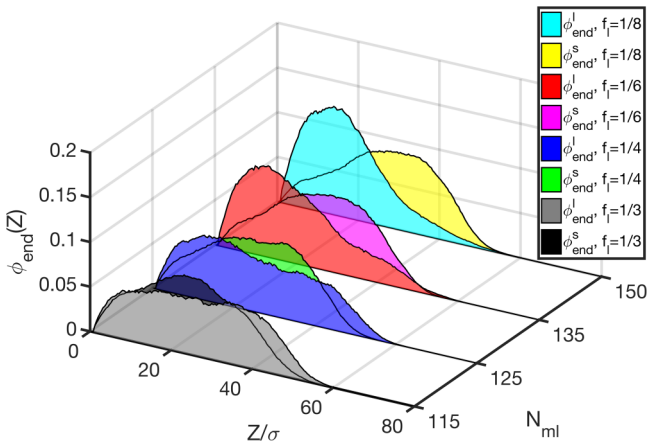

FIG. 5. Probability distributions of free end monomers of grafted linear chains and star chains with different chain lengths and charge fractions of linear chains under the temperature of $T = 2.5\varepsilon$. The linear chain lengths and average charge fractions in the figure correspond to the four phase points in the ideally mixed phase shown in Fig. 3.

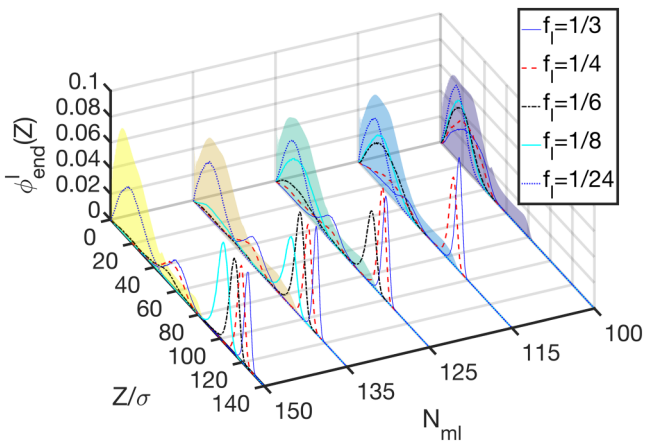

FIG. 6. Normalized probability distributions of free end monomers of grafted linear chains with different chain lengths and charge fractions under a strongly stretching electric field. As in Fig. 2, the overall monomer probability distributions of mixed brushes are shown as the edges of shaded regions in the figure for aiding the identification of the dominant species on the brush surface only. The overall monomer distributions at $f_l = 1/3$ and $1/24$ were chosen to approximate the overall distributions at chain lengths equal to 100 and 150, respectively. For other chain lengths, the overall monomer distributions at the charge fractions corresponding to the ideally mixed phase were selected. The grafting density and degree of substitution in the simulations are $\sigma_g = 0.005$, $R_\alpha = 0.5$.

with the cutoff length of the LJ potential equal to $2^{1/6}\sigma$. Simulations conducted to examine the effect of solvent quality were performed under the poor solvent condition with the cutoff length of the LJ potential equal to 2.5σ. Thus, the Θ temperature is $T_\theta = 3\varepsilon$.[40] It was found that under a temperature of $T \leq 1.5\varepsilon$, the mixed brushes collapse and form bundles. At Θ temperature, the ideally mixed state in the phase diagram shown in Fig. 3 remains unchanged. Nevertheless, it is interesting to find that at a temperature of $T = 2.5\varepsilon$, the effect of solvent quality on the segregation of free end monomers of star and linear chains on the brush surface for mixed brushes in the ideally mixed state is strong. As shown in Fig. 5, at a temperature of $T = 2.5\varepsilon$, with increasing chain length and decreasing charge fraction of grafted linear chains, the probability density distributions of the free end monomers of linear chains shift downward. It can be clearly seen from Fig. 5 and the average height profiles shown in Fig. S4 of the supplementary material that the phase point of $(N_{lm} = 150, f_l = 1/8)$ originally being inside the ideally mixed state is now situated inside the phase of the brush surface dominated by free end monomers of star chains for mixed brushes at a moderately poor solvent condition. Therefore, a moderately poor solvent condition will result in a clockwise rotation of the region of its position of the ideally mixed phase in the phase diagram shown in Fig. 3. The linear chains with a charge fraction of 1/8 are more flexible than star chains with a charge fraction of 1/3 due to weaker electrostatic interaction between charged monomers along the linear chains. Therefore, the linear chains are more susceptible to poor solvent quality and collapse much more strongly than star chains.

D. Mixed brushes under a stretching electric field

Based on the probability distributions of free end monomers of grafted stars and linear chains as shown in Figs. 6 and 7, the phase diagram in terms of the chain length and charge fraction of grafted linear chains, which demarcates different regimes of the dominant species on the brush surface under a strongly stretching electric field ($E = -1.0$), was constructed and is shown in Fig. 8. The phase diagram under a stretching electric field is similar to

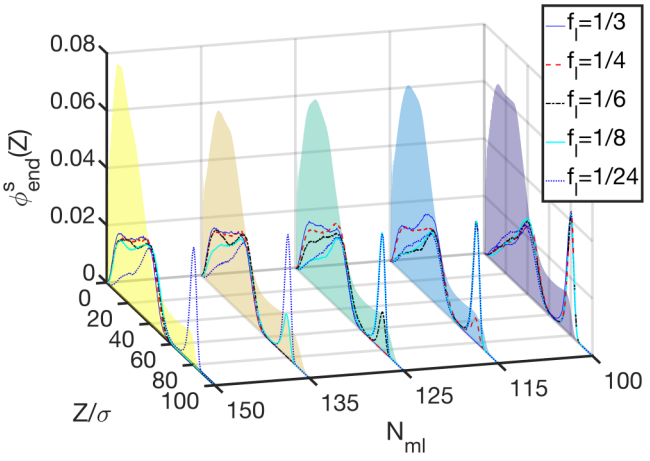

FIG. 7. Normalized probability distributions of free end monomers of grafted 4-arm star chains at different chain lengths and charge fractions of the linear chains under a strongly stretching electric field. Other details regarding the figure are the same as those in Fig. 6.

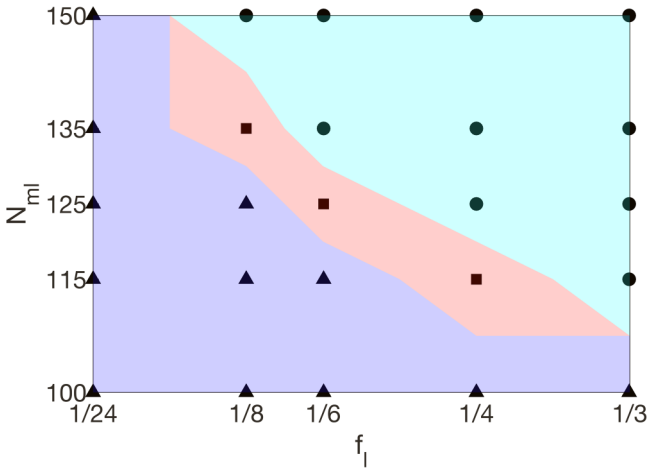

FIG. 8. Phase diagram in terms of the chain length and average charge fraction of linear chains for the mixed brush system under a strongly stretching electric field ($E = -1.0$) depicting different regimes in which end monomers of different species dominate the brush surface. Triangles and spheres indicate the dominance of end groups of grafted stars and linear chains on the brush surface, respectively. Squares correspond to the ideally mixed phase.

that in the absence of external electric fields, both exhibiting three distinctive regimes. Nevertheless, compared with the phase diagram shown in Fig. 3, the regime of an ideally mixed state under a stretching electric field is shifted slightly toward the lower left corner of the phase diagram. Therefore, when the grafted stars and linear chains are in the ideally mixed state in the absence of external electric fields, the linear charged chains are the active component in response to a stretching electric field.

Previous MD simulations of single component PE brushes made of either linear or star chains under a stretching electric field showed that a fraction of grafted chains are strongly stretched and the rest chains are only slightly stretched as revealed by the bimodal probability distributions of end monomers or branching point monomers.[37,41] For the present mixed polyelectrolyte brushes made of linear and star chains under a stretching electric field, we also found that in most cases, the active component also bifurcates into two subpopulations of strongly stretched and very weakly stretched chains with the end monomers of the strongly stretched chains dominating the brush surface. For example, when the linear chains are very short, i.e., $N_{ml} = 100$, or the charge fraction of the linear chains is very low, i.e., $f_l = 1/24$, the end monomers of the active star chains exhibit a bimodal or multimodal distribution, as shown in Fig. 7. Conversely, when the linear chains are long and their charge fraction is high, the probability distributions of the end monomers of the active linear chains are bimodal, as shown in Fig. 6. In certain situations, the probability distribution of the monomers of the inactive component is well separated from that of the weakly stretched chains of the active component (an example is the case of $N_{ml} = 100, f_l = 1/24$ in which the weakly stretched stars reside vertically between the linear chains and strongly stretched stars). In the regime of the ideally mixed state in the phase diagram, each component of the mixed brush bifurcates into two subpopulations, and the distribution of monomers of either strongly stretched or weakly stretched subpopulation of one component overlaps with that of the corresponding subpopulation of the other component (see the curves corresponding to $N_{ml} = 115, f_l = 1/4$, $N_{ml} = 125, f_l = 1/6$, and $N_{ml} = 135, f_l = 1/8$ in Figs. 6 and 7). Thus, mixed brushes in the ideally mixed state under a strongly stretching electric field exhibit a two-layer internal structure.

It was very interesting to find that in the two cases of $N_{ml} = 135, f_l = 1/6$ (see Fig. 6) and $N_{ml} = 150, f_l = 1/12–1/8$ (see Figs. 6 and 9), the end monomers of linear chains, which are the active component in the mixed brush, exhibit only a single mode probability distribution. As shown in Fig. 9, at the lowest charge fraction of $f_l = 1/24$, the linear chains with a chain length of 150 are the inactive component and reside at the bottom of the brush layer. At $f_l = 1/15$, the linear chains become the active component and the brush surface is dominated by the end monomers of the linear chains. When the charge fraction is increased to $f_l = 1/12–1/8$, the probability distribution of the end monomers of the linear chains has only a single peak. Such a conformational transition of the linear chains in the mixed polyelectrolyte brushes induced by the charge fraction of the linear chains is similar to the so-called "coil-to-flower" conformational transition in a single "minority" linear neutral polymer chain inserted into a neutral polymer brush made of star macromolecules perturbed by either the length of linear chain or the brush grafting density proposed by Polotsky.[32] If the charge fraction is further increased, the active linear chains bifurcate into two subpopulations with the strongly stretched subpopulation decreasing in population weight and moving to larger height. Such a unique feature of a single mode

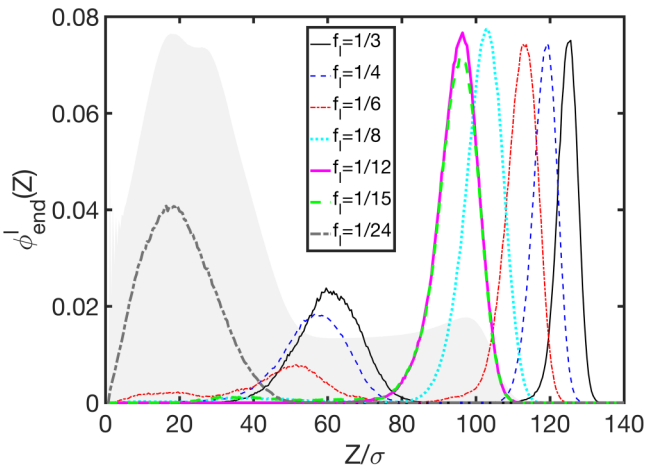

FIG. 9. The probability distributions of end monomers of linear chains with a chain length of 150 at different charge fractions shown as legends inside the figure under a strongly stretching electric field are displayed, some of which are also shown in Fig. 6 (charge fraction $f_l = 1/3, 1/4, 1/6, 1/8, 1/24$ at $N_{ml} = 150$). The external boundary of the gray background is the probability distribution of all of monomers in the mixed brush system. The grafting density and degree of substitution in the simulations are $\sigma_g = 0.005$, $R_\alpha = 0.5$.

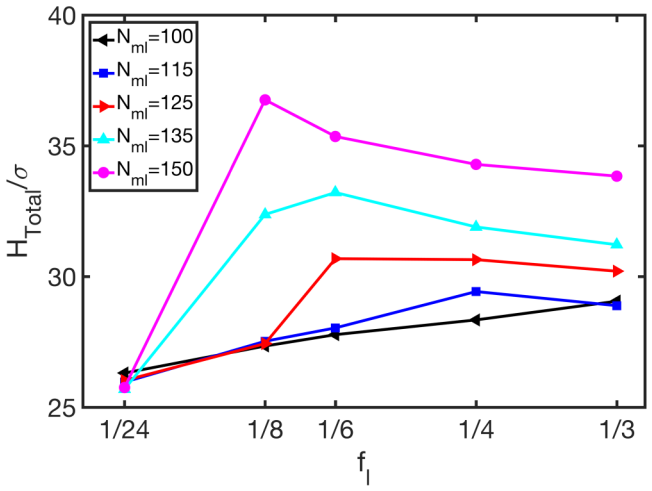

FIG. 10. Center of mass heights of mixed brushes as functions of average charge fraction of linear chains at different chain lengths of linear chains under strongly stretching electric fields.

distribution of the end monomers of stretched linear chains has an impact on the center of mass height of mixed brushes. As shown in Fig. 10, for mixed brushes with linear chain lengths of 135 and 150, the center of mass heights varies with the charge fraction of linear chains in a clearly nonmonotonic fashion. The peaks of the two curves with $N_{ml} = 135, 150$ correspond to the single mode distributions of the end monomers of stretched linear chains. When the charge fraction is further increased beyond the value corresponding to the peak, the active linear chains bifurcate into two subpopulations with the less stretched population increasing in population weight, and the star chains become the inactive component and retract toward the grafting substrate, leading to the decrease of the center of the mass height of mixed brushes with increasing charge fraction.

The stratification within the brush layer was examined. The fractions of stretched grafted linear chains R^L_{up} and star chains R^S_{up} were used to quantify the degree of stratification. If the probability distribution of end monomers of linear chains or stars exhibits two peaks separated by a trough with zero amplitude, the population weight of the mode at larger height is defined as R^L_{up} (R^S_{up}). On the other hand, if end monomers exhibit a somewhat unimodal distribution and the distribution is well buried deep inside the brush layer, $R^L_{up}(R^S_{up})$ was set to zero. For a unimodal distribution of the end monomers centered near the brush surface, the corresponding value of $R^L_{up}(R^S_{up})$ was set to 1. The effects of the length and charge fraction of linear chains on the stratification of mixed brushes under a strongly stretched electric field are shown in Fig. 11. The trends shown in Fig. 11 are well correlated to the phase diagram shown in Fig. 8. In the regime of the brush surface dominated by the end monomers of stars (the lower left part of the phase diagram), the linear chains reside at the bottom of the brush layer. Thus, R^L_{up} is zero. As the charge fraction of linear chains increases, the mixed brush enters the ideal mixing state accompanied by the rapid increase of R^L_{up} and rapid decrease of R^S_{up}. In the regime corresponding to the upper right part of the phase diagram, the fraction of stretched star chains drops to zero. It can be further seen from Fig. 11 that, in the regime of the brush surface dominated by the end monomers of stars, the fraction of stretched stars is quite insensitive to changes in the charge fraction of linear chains. Furthermore, Fig. 11 shows that R^L_{up} of linear chains dominating the brush surface is much larger than R^S_{up} of star chains dominating the brush surface.

E. Mixed brushes under a strongly collapsing electric field

Under a strongly collapsing electric field, the charged linear and star chains compete with each other for neutralizing the oppositely

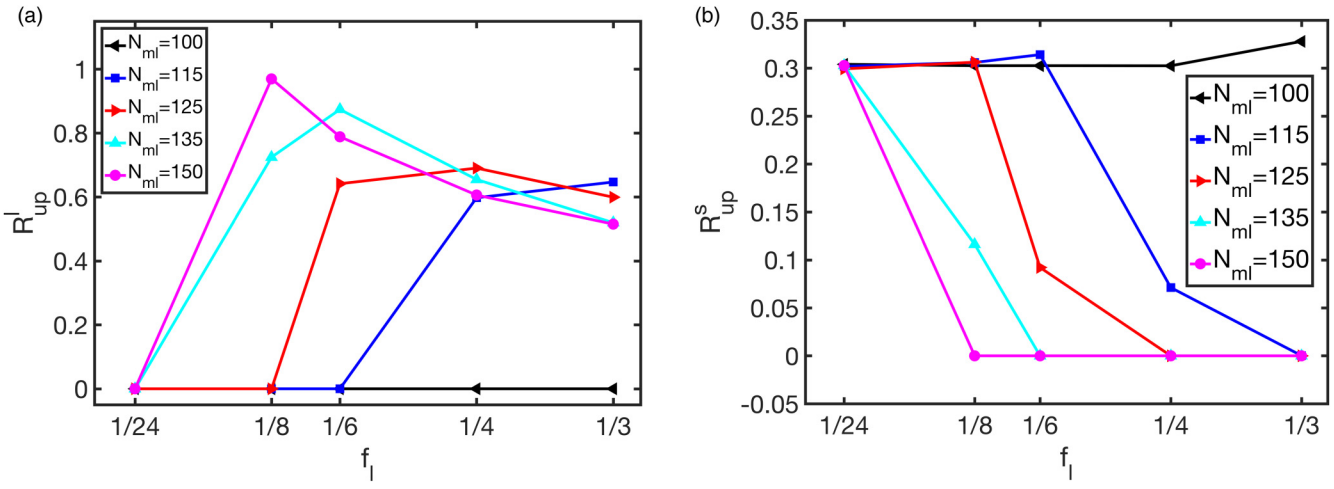

FIG. 11. The fractions of stretched linear (a) and star (b) chains under an electric field as functions of the charge fraction of linear chains at different linear chain lengths.

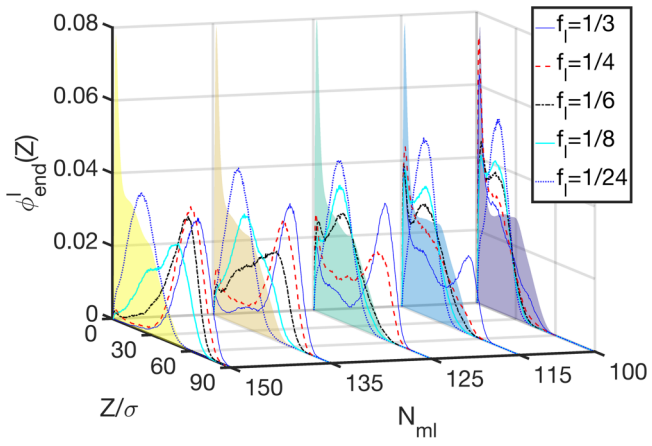

FIG. 12. Normalized probability distributions of free end monomers of grafted linear chains with different chain lengths and charge fractions under a collapsing electric field. The overall monomer probability distributions of mixed brushes are shown as the edges of shaded regions in the figure for aiding the identification of the dominant species on the brush surface only. The grafting density and degree of substitution in the simulations are $\sigma_g = 0.005$, $R_\alpha = 0.5$.

charged grafting electrode. Because in this study a grafted star chain carries more charges than a linear chain, the star chains are more likely to be attracted to the grafting electrode than linear chains. On the other hand, if the linear chains are short, they prefer to reside near the grafting electrode. Such a competition would give rise to interesting conformations of mixed polyelectrolyte brushes under a collapsing electric field. With the aid of the probability distributions of end monomers of both the linear chains and 4-arm star chains shown in Figs. 12 and 13, the phase diagram was constructed and is shown in Fig. 14. As shown in Fig. 14, the lower left region of the phase diagram in the absence of external electric fields is divided into two regimes under a strongly collapsing electric field. If the charge fraction of linear chains is very low (the leftmost part of the phase diagram with $f_l = 1/24$), a fraction of charged stars collapse and reside at the bottom of the brush layer as revealed by the strong and sharp peaks in the immediate vicinity of the grafting electrode corresponding to $f_l = 1/24$ shown in Fig. 13, pushing the linear chains upward. Thus, the linear chains are in the middle of the vertical brush layer (see the unimodal distributions of the end monomers of the linear chains at $f_l = 1/24$ in Fig. 12) and the rest of the stars are located in the upper layer, effectively creating a three-layer structure, which is absent for mixed brushes in the absence of external electric fields and in a strongly stretching electric field. Note that there are always some charged stars collapsing onto the grafting electrode due to the larger amount of charges carried by stars compared with the linear chains (see the sharp peaks near the grafting electrode shown in Fig. 13), leading to bimodal or multimodal distributions of the end monomers of 4-arm stars. For example, in the case of $N_{ml} = 100$, $f_l = 1/3$, although the bottom of the brush layer is dominated by the collapsed linear chains, there is a small fraction of collapsed stars in the immediate vicinity of the grafting electrode (see Fig. 13). It can be clearly seen by comparing Fig. 3 with Fig. 14 that the ideal mixing regime and the regime corresponding to the brush surface dominated by the end monomers of linear chains are not affected much by a collapsing electric field. It is evident from Figs. 12 and 13 that for the three phase points located in the ideal

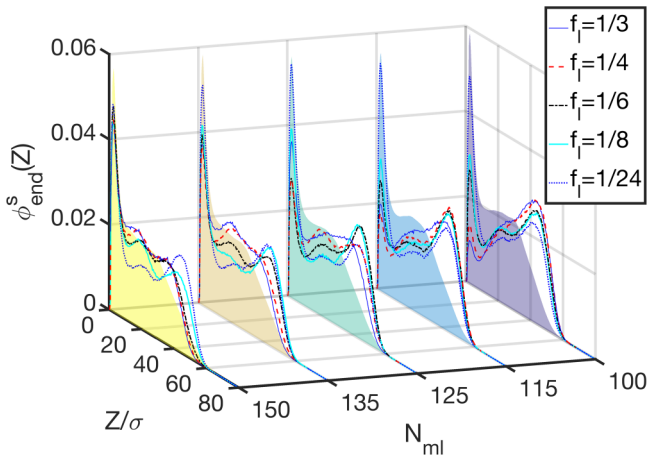

FIG. 13. Normalized probability distributions of free end monomers of grafted 4-arm star chains at different chain lengths and charge fractions of the linear chains under a collapsing electric field. The grafting density and degree of substitution in the simulations are $\sigma_g = 0.005$, $R_\alpha = 0.5$.

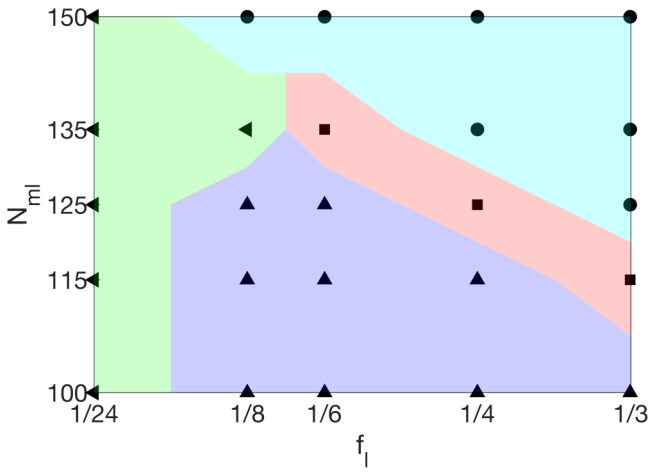

FIG. 14. Phase diagram in terms of the chain length and average charge fraction of linear chains for the mixed brush system under a strongly collapsing electric field ($E = 1.0$) depicting different regimes in which end monomers of different species dominate the brush surface. Up-pointing triangles and spheres indicate the dominance of end groups of grafted stars and linear chains on the brush surface, respectively. Squares correspond to the ideal mixing phase in which both the end monomers of linear and star chains exist on the brush surface. In the regime on the left side of the phase diagram with left-point triangles, a fraction of grafted star chains reside at the bottom of the brush layer and the rest of the star chains are in the upper layer with the grafted linear chains sandwiched between them, effectively creating a three-layer structure.

mixing phase, i.e., $N_{ml} = 115, f_l = 1/3$, $N_{ml} = 125, f_l = 1/4$ and $N_{ml} = 135, f_l = 1/6$, the probability distributions of the free end monomers of the linear chains and star chains significantly overlap with each other in the whole vertical region of the mixed brushes.

The degree of stratification within the brush layer under a strongly collapsing electric field was examined by quantitatively analyzing the fraction of collapsed linear chains and stars R^L_{down}/R^S_{down}. Unlike mixed brushes under a strongly stretching field, the two/multiple modes in the probability distribution of end monomers of linear chains or stars under a collapsing electric field strongly overlap with each other. R^L_{down} and R^S_{down} are defined as follows. If the linear chains collapse under an electric field, a sharp peak emerges in the probability distribution of end monomers in the immediate vicinity of the grafting electrode. The area under the curve of normalized probability distribution in the interval of $[0 \le z \le h_l]$ is defined as R^L_{down}, where h_l denotes the vertical position of the starting point of the plateau on the right side of the peak near the grafting electrode. For grafted stars, the area under the curve of normalized probability distribution of the branching points in the internal of $[0 \le z \le h_s]$ is defined as R^S_{down}, where h_s denotes the vertical position of the trough of the probability distribution. As shown in Fig. 15, for the case of relatively short linear chains, the overall trend is that the fraction of collapsed linear chains gradually increases with increasing charge fraction of linear chains, whereas the fraction of collapsed stars decreases with increasing charge fraction of linear chains. On the other hand, for mixed brushes with very long linear chains ($N_{ml} = 150$), collapsed stars are the sole charge neutralizer for the opposite surface charges on the grafting electrode and R^S_{down} is insensitive to change in the charge fraction of linear chains.

Under a strongly collapsing electric field, a fraction of linear and/or star chains are adsorbed onto the oppositely charged grafting electrode. It was found from simulations that charge overcompensation takes place for collapsed charged monomers; that is, the amount of charges on collapsed monomers exceeds that of surface charges on the grafting electrode. A salient feature of the emergence of charge overcompensation in the immediate vicinity of the grafting electrode is that some counterions with the same charge sign as the surface charges are also attracted toward the grafting electrode in order to establish an overall charge neutrality near the grafting electrode. In order to define the degree of charge overcompensation Ξ, the adsorption layer near the grafting electrode was identified first. In the immediate vicinity of the grafting electrode, there is a sharp peak in the probability distribution of charged monomers, which is above the corresponding distribution in the absence of electric fields. The vertical position of the point at which these two normalized probability distributions intersect with each other can be found. The region from $z = 0$ to the z coordinate of the intersection point was labeled as the adsorption layer. Then, the degree of charge overcompensation Ξ can be computed from the following expression:

$$\Xi = \frac{N_c(\beta_1 - \beta_0)}{s\sigma_e} - 1, \tag{1}$$

with s denoting the average surface area occupied by one grafted chain ($s = 1/\sigma_g$), $N_c = f_l N_{ml} R_\alpha + 4N_{ms} f_s (1 - R_\alpha)$ defining the average number of elementary charges carried by a grafting chain, and β_1, β_0 denoting the areas under the normalized probability distributions of charged monomers in the interval spanned by the adsorption layer at $E = 1.0, 0$, respectively. In the above equation, σ_e is the surface charge density on the two oppositely charged electrodes ($\sigma_e = \varepsilon_0 \varepsilon_r |\vec{E}|$ in an SI unit with $\varepsilon_0, \varepsilon_r$ denoting the vacuum permittivity and dielectric constant of water, respectively). It is easy to show that using dimensionless parameters, the degree of charge overcompensation is

$$\Xi = 4.8\pi \cdot (\lambda_B/\sigma) \cdot \sigma_g^* \cdot N_c \cdot (\beta_1 - \beta_0)/E - 1. \tag{2}$$

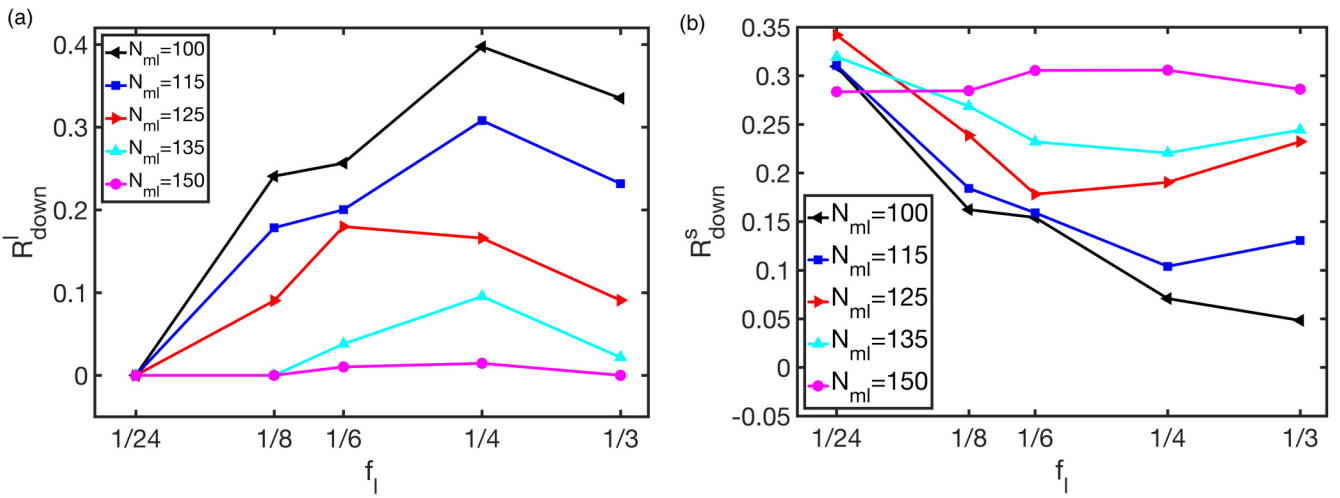

FIG. 15. Fractions of collapsed linear chains (a) and stars (b) as functions of the charge fraction of linear chains at different linear chain lengths.

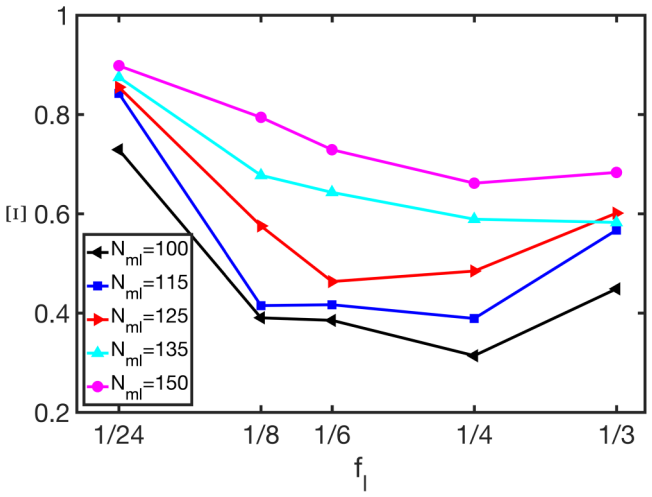

FIG. 16. Degrees of charge overcompensation as functions of charge fraction of linear chains at different linear chain lengths.

The degree of charge overcompensation was quantified, and its dependences on the chain length and charge fraction of linear chains are illustrated in Fig. 16. It can be seen from Fig. 16 that, for short linear chains ($N_{ml} = 100$), the degree of charge overcompensation in the regime dominated by adsorbed stars (at $f_l = 1/24$) is higher than that in the regime dominated by adsorbed linear chains (at $f_l = 1/3$). This is because a star carries more charges ($\sim 4 \times 50/3$) than a linear chain ($100/3$), resulting in stronger charge neutralizing ability of stars compared with linear chains. When both types of chains contribute significantly to charge compensation (at $f_l \in [1/8, 1/4]$ and $N_{ml} \in [100 - 125]$), the resulting degree of charge overcompensation is smaller than those in the other two scenarios. Furthermore, for the case of the longest linear chains in which the stars contribute solely to charge compensation, the highest degree of charge overcompensation is achieved.

IV. CONCLUSION

In this work, we have performed Langevin dynamics simulations to study the conformations and stratification in mixed polyelectrolyte brushes composed of linear chains and 4-arm stars in response to changes in length and average charge fraction of linear chains, Bjerrum length, the solvent quality as well as external electric fields. Through detailed analysis of heights of center of mass of brushes, probability distributions of end monomers of linear chains and stars as well as the branching points of stars, fractions of stretched/collapsed linear chains and stars, and degree of charge overcompensation, phase diagrams in terms of the length and charge fraction of linear chains demarcating different regimes of the composition of brush surfaces were constructed under different external electric fields. Our simulation study showed that compared with external electric fields, changing Bjerrum length or the solvent quality is less effective in tuning the surface switching properties of mixed polyelectrolyte brushes made of star and linear chains. Simulation results revealed that under a strongly stretching electric field or in the absence of electric fields, there exist three different regimes in the phase diagram in terms of the length and charge fraction of linear chains. In the lower left part of the phase diagram, the end monomers of stars dominate the brush surface and the linear chains reside at the bottom of the brush layer. In the upper right part of the phase diagram, the end monomers of stretched linear chains are the dominating species on the brush surface. Between these two regimes, there exists the ideally mixed state. However, when the mixed brushes experience a strongly collapsing electric field, besides the above three different regimes, a new regime emerges in the leftmost side of the phase diagram, in which the linear chains reside in the middle of the brush layer between the strongly collapsed stars and noncollapsed stars.

SUPPLEMENTARY MATERIAL

See the supplementary material for methodological details (Sec. I), average heights of the free end monomers of grafted star and linear chains as a function of the linear chain length under the condition of $\lambda_B = 10\sigma$ (Fig. S1), normalized probability density distributions of free end monomers of grafted star and linear chains of the mixed brushes at $\lambda_B = 0.5\sigma$ (Fig. S2), average heights of free end monomers of grafted star and linear chains of the mixed brushes at $\lambda_B = 0.5\sigma$ (Fig. S3), and average heights of free end monomers of grafted star and linear chains of the mixed brushes at $T = 2.5\varepsilon$ (Fig. S4).

ACKNOWLEDGMENTS

The authors acknowledge the financial support from the National Natural Science Foundation of China (NNSFC Project No. 21774067). C.T. acknowledges the support from K. C. Wong Magna Fund in Ningbo University.

REFERENCES

[1]D. H. Napper, *Polymer Stabilization of Colloidal Dispersions* (Academic Press, New York, 1983).
[2]G. J. Fleer, M. A. Cohen Stuart, J. M. H. M. Scheutjens, T. Cosgrove, and B. Vincent, *Polymers At Interfaces* (Chapman & Hall, London, 1993).
[3]W. L. Chen, R. Cordero, H. Tran, and C. K. Ober, Macromolecules **50**, 4089 (2017).
[4]A. Wittemann, B. Haupt, and M. Ballauff, Phys. Chem. Chem. Phys. **5**, 1671 (2003).
[5]M. P. Weir, S. Y. Heriot, S. J. Martin, A. J. Parnell, S. A. Holt, J. R. P. Webster, and R. A. L. Jones, Langmuir **27**, 11000 (2011).
[6]I. Szleifer and M. A. Carignano, Adv. Chem. Phys. **94**, 165 (1996).
[7]S. T. Milner, T. A. Witten, and M. E. Cates, Macromolecules **21**, 2610–2619 (1988).
[8]A. Halperin, M. Tirrell, and T. P. Lodge, Adv. Polym. Sci. **100**, 31–71 (1991).
[9]A. Naji, C. Seidel, and R. R. Netz, Adv. Polym. Sci. **198**, 149–183 (2006).
[10]S. Das, M. Banik, G. Chen, S. Sinha, and R. Mukherjee, Soft Matter **11**, 8550–8583 (2015).
[11]O. V. Borisov, E. B. Zhulina, and T. M. Birshtein, Macromolecules **27**, 4795–4803 (1994).
[12]R. R. Netz and D. Andelman, Phys. Rep. **380**, 1–95 (2003).
[13]P. Pincus, Macromolecules **24**, 2912 (1991).
[14]R. Israels, F. A. M. Leermakers, G. J. Fleer, and E. B. Zhulina, Macromolecules **27**, 3249–3261 (1994).

[15]N. V. Brilliantov, Y. A. Budkov, and C. Seidel, Phys. Rev. E **93**, 032505 (2016).
[16]E. B. Zhulina, T. M. Birshtein, and O. V. Borisov, Macromolecules **28**, 1491–1499 (1995).
[17]P. Romiszowski and A. Sikorski, J. Chem. Inform. Comp. Sci. **44**, 393–398 (2004).
[18]A. A. Polotsky, T. Gillich, O. V. Borisov, F. A. M. Leermakers, M. Textor, and T. M. Birshtein, Macromolecules **43**, 9555 (2010).
[19]A. A. Polotsky, F. A. M. Leermakers, E. B. Zhulina, and T. M. Birshtein, Macromolecules **45**, 7260–7273 (2012).
[20]H. Merlitz, C. X. Wu, and J. U. Sommer, Macromolecules **44**, 7043 (2011).
[21]H. Merlitz, W. Cui, C. X. Wu, and J. U. Sommer, Macromolecules **46**, 1248 (2013).
[22]C. W. Li, H. Merlitz, C. X. Wu, and J. U. Sommer, Polymer **98**, 437 (2016).
[23]O. V. Borisov, A. A. Polotsky, O. V. Rud, E. B. Zhulina, F. A. M. Leermakers, and T. M. Birshtein, Soft Matter **10**, 2093 (2014).
[24]E. B. Zhulina, V. M. Amoskov, A. A. Polotsky, and T. M. Birshtein, Polymer **55**, 5160 (2014).
[25]O. V. Borisov, E. B. Zhulina, A. A. Polotsky, F. A. M. Leermakers, and T. M. Birshtein, Macromolecules **47**, 6932 (2014).
[26]E. B. Zhulina, F. A. M. Leermakers, and O. V. Borisov, Langmuir **31**, 6514 (2015).
[27]W. Cui, C. F. Su, H. Merlitz, C. X. Wu, and J. U. Sommer, Macromolecules **47**, 3645 (2014).
[28]O. V. Borisov and E. B. Zhulina, Macromolecules **48**, 1499 (2015).
[29]J. S. Kłos and J. U. Sommer, Macromolecules **48**, 1179 (2015).
[30]K. Miliou, L. N. Gergidis, and C. Vlahos, J. Polym. Sci. B Polym. Phys. **55**, 1110 (2017).
[31]A. A. Polotsky, F. A. M. Leermakers, and T. M. Birshtein, Macromolecules **48**, 2263 (2015).
[32]A. A. Polotsky, A. D. Kazakov, and T. M. Birshtein, Polymer **130**, 242 (2017).
[33]C. F. Su, H. Merlitz, C. X. Wu, and J. U. Sommer, J. Chem. Phys. **145**, 234905 (2016).
[34]I. C. Yeh and M. L. Berkowitz, J. Chem. Phys. **111**, 3155 (1999).
[35]U. Essmann, L. Perera, M. L. Berkowitz, T. Darden, H. Lee, and L. G. Pedersen, J. Chem. Phys. **153**, 8577 (1999).
[36]H. D. Ding, C. Duan, and C. H. Tong, J. Chem. Phys. **146**, 034901 (2017).
[37]Y. F. Ho, T. N. Shendruk, G. W. Slater, and P. Y. Hsiao, Langmuir **29**, 2359–2370 (2013).
[38]M. J. Stevens and K. Kremer, J. Chem. Phys. **103**, 1669 (1995).
[39]J. F. Kolb, R. P. Joshi, S. Xiao, and K. H. Schoenbach, J. Phys. Appl. Phys. **41**, 234007 (2008).
[40]G. S. Grest and M. Murat, Macromolecules **26**, 3108 (1993).
[41]F. Zhang, S. Y. Wang, H. D. Ding, and C. H. Tong, Soft Matter **15**, 2560–2570 (2019).